High-throughput hyperspectral phenotyping and transcriptomics reveal expression networks associated with nitrogen-limitation-induced senescence in sorghum

Mohammad B. Belaffif
HudsonAlpha Institute for Biotechnology
Mackenzie Zwiener-Malcom
University of Nebraska-Lincoln
Avinash Sreedasyam
HudsonAlpha Institute for Biotechnology
Gopal Battu
HudsonAlpha Institute for Biotechnology
Zhongjie Ji
University of Nebraska-Lincoln
Pradeepa Hirannaiah
HudsonAlpha Institute for Biotechnology
Shilpa Manjunatha
HudsonAlpha Institute for Biotechnology
Marcin Grzybowski
University of Nebraska-Lincoln
Salema Myler
HudsonAlpha Institute for Biotechnology
Blake Dietz
HudsonAlpha Institute for Biotechnology
Jane Grimwood
HudsonAlpha Institute for Biotechnology
Yufeng Ge
University of Nebraska-Lincoln
Jeremy Schmutz
HudsonAlpha Institute for Biotechnology
James C. Schnable
University of Nebraska-Lincoln

Kankshita Swaminathan

kswaminathan@hudsonalpha.org

HudsonAlpha Institute for Biotechnology

Research Article

Keywords: Sorghum, nitrogen remobilization, leaf senescence, hyperspectral phenotyping, gene regulatory network

Posted Date: June 10th, 2026

DOI: https://doi.org/10.21203/rs.3.rs-9954680/v1

Additional Declarations: No competing interests reported.

High-throughput hyperspectral phenotyping and transcriptomics reveal expression networks associated with nitrogen-limitation-induced senescence in sorghum.

List of Authors

Mohammad B. Belaffif[1,2,3*], Mackenzie Zwiener-Malcom[4*], Avinash Sreedasyam[1*], Gopal Battu[1,2], Zhongjie Ji[4], Pradeepa Hirannaiah[1,2], Shilpa Manjunatha[1,2], Marcin Grzybowski[4,5], Salema Myler[1], Blake Dietz[1], Jane Grimwood[1], Yufeng Ge[4], Jeremy Schmutz[1], James C. Schnable[4], Kankshita Swaminathan[1,2#]

Institutional affiliations

[1]HudsonAlpha Institute for Biotechnology, 601 Genome Way, Huntsville, AL 35806, USA
[2]Center for Advanced Bioenergy and Bioproducts Innovation, 1206 W. Gregory Drive (IGB), Urbana, IL 61801, USA
[3]Agria Analytica, CIBIS NINE 11th Floor, Jl.TB Simatupang No. 2, Jakarta Selatan, DKI Jakarta 12560, Indonesia
[4]University of Nebraska-Lincoln, Lincoln, NE, USA
[5]Institute of Plant Experimental Biology and Biotechnology, Faculty of Biology, University of Warsaw, Warsaw, Poland.

* These authors contributed equally to this work

[#] Corresponding author

Contact information

Kankshita Swaminathan <kswaminathan@hudsonalpha.org>

Abstract

Background: Sorghum (*Sorghum bicolor*) is a versatile C4 crop used for food and feed and as biomass for bioproducts and energy. Improving nitrogen use efficiency (NUE) in sorghum is important because fertilizer is costly and excessive fertilizer use has negative environmental impacts. Leaf senescence mediates nutrient recycling, but its dynamic progression is difficult to quantify at scale. We evaluated whether visible-near-infrared hyperspectral imaging can provide high-throughput measures of N-limitation-induced senescence in sorghum and link these phenotypes to gene expression. Sorghum Tx430 plants were grown under four N treatments (6, 9, 12, and 15 mM), imaged from vegetative growth through grain fill, and destructively sampled for RNA-seq at four developmental stages.

Results: A supervised support vector machine with a radial basis function kernel classified pixels from a hyperspectral image of sorghum plants grown under different N levels into green leaf, yellow leaf, dry leaf, stalk, panicle, and background classes with 0.93 accuracy. We defined the senescence ratio as the sum of yellow and dry leaf areas divided by the green leaf area and computed it across multiple growth stages and nitrogen levels. The senescence ratio did not differ among N treatments during vegetative growth, but it declined with increasing N during boot, anthesis, and grain fill, indicating earlier senescence under N limitation. Among the genes whose expression positively correlated with senescence ratio were 13 putative transcription factors, including SbiRTX430.02G247100, a WRKY1/ZAP1 homolog and a WRKY4 homolog. Gene regulatory network analysis of the top 1% of genes associated with SbiRTX430.02G247100 showed enrichment for processes associated with leaf senescence and chlorophyll catabolism. In contrast, the network associated with the WRKY4 homolog was enriched for autophagy-related terms.

Conclusions: Our study shows that automated hyperspectral imaging is highly effective for monitoring dynamic plant phenotypes, such as stress-induced senescence, that are difficult to visually score with the naked eye. Here, nitrogen deficiency served as the stress condition. Still, this approach supports large-scale phenotypic data collection for any such stressor and enables analyses with greater statistical power, yielding more robust conclusions and the potential for new insights that can be applied to engineering and breeding better crops.

Keywords

Sorghum; nitrogen remobilization; leaf senescence; hyperspectral phenotyping; gene regulatory network

Graphical abstract

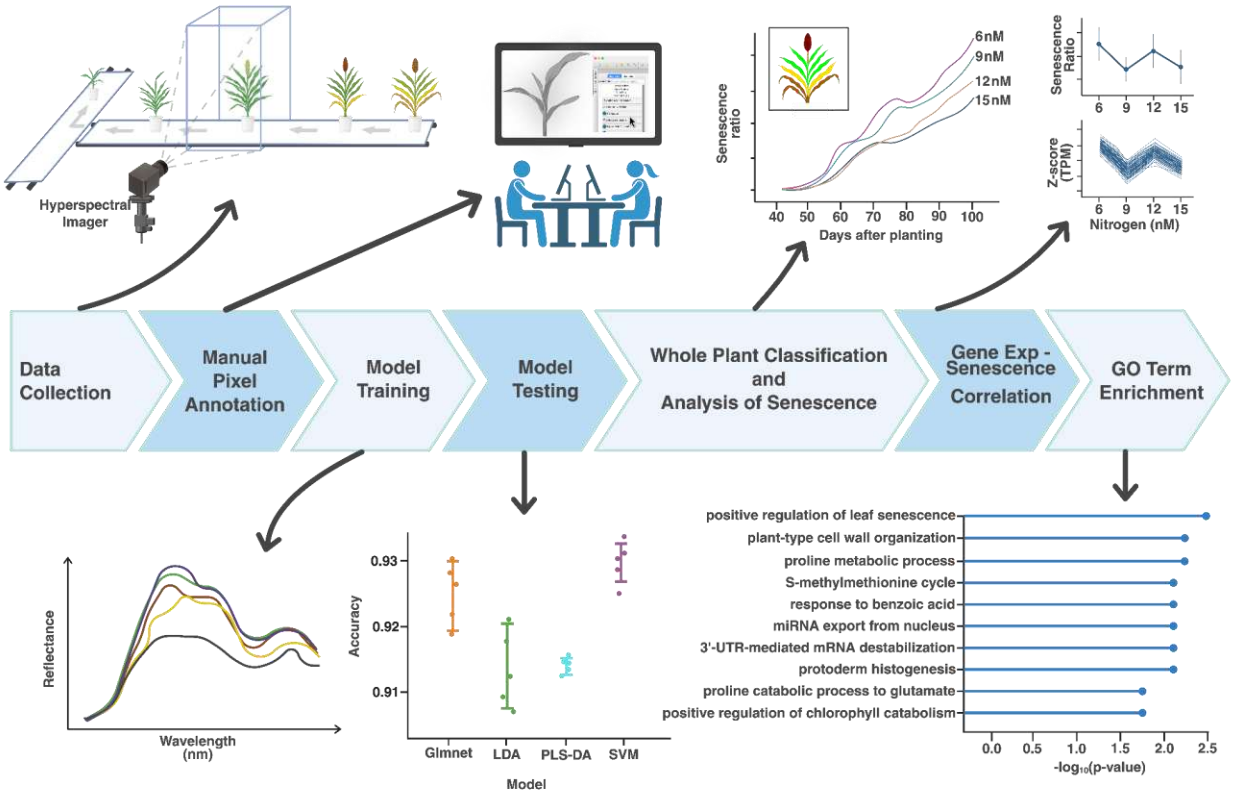

GRAPHICAL ABSTRACT: Sorghum plants grown under varying Nitrogen conditions were photographed in visible and hyperspectral wavelengths on a high-throughput phenotyping platform. These images were used for model training followed by testing, plant tissue classification, pixel-based senescence quantification, and gene expression analysis. Created in https://BioRender.com

Background

Nitrogen is a key macronutrient for plants and is essential for the synthesis of basic biochemical building blocks such as amino acids, nucleic acids, and chlorophyll. Hence, it is critical for crop growth and development. Since it limits growth and productivity, nitrogen is routinely supplemented as chemical or organic fertilizer in modern agriculture to boost yields. Unfortunately, only 50–75% of the nitrogen applied is taken up and incorporated in the plant, with the remainder lost via leaching, volatilization, nitrification, denitrification, and drainage (Garnier et al., 2023; Govindasamy et al., 2023; Mălinaş et al., 2022). This difference between the nitrogen applied and the nitrogen incorporated is both economically expensive for the farmer and environmentally detrimental.

Nitrogen use efficiency (NUE) is a key agronomic metric that describes how effectively crops take up, assimilate, and allocate nitrogen to support growth and development, ultimately affecting biomass and grain yields. Comparisons between high-NUE and low-NUE lines have revealed measurable phenotypic differences in growth, development, greenness, yield, and other physiological measurable traits (Gu et al., 2025; Liang et al., 2023). Improving NUE to reduce fertilizer inputs while maintaining crop productivity is thus a major focus for agronomically important crops and has become more urgent under increasingly variable environmental conditions and depleted soils (Chen et al., 2020; Congreves et al., 2021). NUE is commonly partitioned into nitrogen uptake efficiency, nitrogen assimilation efficiency, and nitrogen remobilization efficiency. Of these, nitrogen remobilization is especially important during reproductive development, when nitrogen stored in vegetative tissues is redistributed to developing grains and other sink organs, such as rhizomes where applicable. In cereals, remobilized nitrogen can account for a substantial fraction of grain nitrogen, with estimates of 50–70% in wheat (Barneix, 2007), up to 90% in some wheat and rice studies (Hajibarat & Saidi, 2022), and 35–55% in maize (Hirel et al., 2005). Despite its importance, nitrogen remobilization efficiency remains comparatively difficult to study at scale because accurate quantification often requires destructive sampling, tissue nitrogen measurements, or isotope-based approaches such as ^{15}N labeling. These technical constraints have limited large-scale phenotyping and genetic dissection of remobilization-associated traits, particularly in systems where senescence dynamics vary across developmental stage, genotype, and nitrogen availability (Chen et al., 2020; Liang et al., 2023).

Nitrogen remobilization is crucial during the reproductive stage. During this stage, plants rely on nitrogen reserves stored in vegetative tissues, such as leaves, to feed seeds and maximize reproductive success, making senescence a key process associated with NUE and grain yield (Doan et al., 2024). An intricate regulatory network of hormonal cues, environmental stimuli and stresses like drought and nutrient limitations, and age-related signals govern senescence. Early senescence under stress conditions will shunt nitrogen from the oldest leaves to the youngest, leading to premature flowering and poor yields. On the opposite end of the spectrum are "stay green" traits, where nitrogen stored in the leaves as photosynthetic proteins results in more green leaves and delayed flowering. Phytohormones and many transcription factors, especially those in the NAC and WRKY families, play a central role in regulating senescence, and nitrogen

deficiency has been shown to upregulate amino-acid transporters and proteases (Breeze et al., 2011; Hajibarat & Saidi, 2022). High NUE lines in *Brassica napus* show enhanced senescence and yield under low nitrogen (Liang et al., 2023), suggesting the importance of nitrogen remobilization in maintaining plant fitness. In Arabidopsis, nitrogen remobilization occurs independently of nitrogen uptake, with stored nitrogen redistributed during reproductive development to meet increased nitrogen demand, as the rate of nitrogen uptake from the environment is significantly reduced at this stage compared to the vegetative stage (Masclaux-Daubresse et al., 2010). This underscores the importance of nitrogen remobilization in ensuring plant fitness and yield.

Sorghum bicolor is a great multipurpose crop especially known for its ability to thrive and yield in arid regions with poor soils (Gardner et al., 1994; Gelli et al., 2017; Hao et al., 2014; Propheter & Staggenborg, 2010; Rooney et al., 2007; Zheng et al., 2023). Its adaptability to marginal lands, the availability of lines bred for multiple uses (food, feed, biomass for energy) combined with the availability of extensive genetic, genomic, and phenomic resources, makes it a perfect crop for studying genotype-environment interactions to enable further improvement and breeding (Baloch et al., 2023; Boatwright et al., 2022; LeBauer et al., 2020). The grain sorghum genotype *S. bicolor* 'RTx430' was selected as the primary genotype for this study on the transcriptomics networks associated with senescence in response to nitrogen availability because of its suitability for *Agrobacterium*-mediated transformation (Liu & Godwin, 2012) and availability of a high-quality reference genome (Deschamps et al., 2018).

Gene Regulatory Networks (GRNs) are a map of complex interactions between regulatory hubs like transcription factors and micro RNAs and their target genes (Mercatelli et al., 2020). Thus GRNs offer insights into molecular responses associated with environmental cues and developmental and physiological effects. The molecular mechanisms of senescence remain poorly understood due to the complexity of the GRNs that control it (Woo et al., 2018). Genetic diversity and crosstalk between factors like developmental age and external factors like nutrient status and stress that can trigger the onset of senescence (Doan et al., 2024) pose a challenge in identifying GRNs regulating senescence in general and nitrogen remobilization in particular.

Temporally resolved phenotyping alongside transcriptomics can enable the reconstruction of GRNs for traits like senescence, which influences NUE, harvest index, and grain protein content (Gaju et al., 2014; Gregersen et al., 2008; Liang et al., 2023; Shanks et al., 2022; Yang & Zhang, 2006). Traditional methods like visual inspection or SPAD chlorophyll measurements are difficult to scale across genotypes and environments (Anderegg et al., 2019) but spectral imaging is an alternative that can be measured at scale. Spectral imaging works by capturing the spectral intensity at wavelengths associated with pigments, canopy structure, and water status. In plant phenotyping, visible, near-infrared, short-wave infrared, thermal, and chlorophyll fluorescence measurements are used for related but distinct traits. Such imaging has been used to detect disease, heavy-metal stress, plant water status, and nitrogen status (Ram et al., 2024). Hyper spectral imaging (HSI) was shown to be accurate and scalable in wheat and chickpea for senescence (Anderegg et al., 2019; Cai et al., 2016) and more recently used to study the N response of sorghum mutants, generated by gene editing (Jin et al. 2025).

Here, we tested whether visible-near infrared hyperspectral imaging could quantify N-responsive leaf senescence in sorghum under varying N conditions. We trained machine learning classifiers to segment sorghum tissue classes and derive a pixel-based senescence ratio. We then integrated this phenotype with RNA-seq profiles from leaves sampled across N treatments and developmental stages to identify genes and candidate regulatory networks associated with senescence and N remobilization.

Methods

Plant growth and nitrogen application

Sorghum line Tx430 was selected as the primary genotype for this study. To increase the generalizability of the machine learning models described below, and capture the genotypic and phenotypic diversity within sorghum, nine additional genetically diverse lines from the Sorghum Association Panel (SAP) were included for training purposes: SC85, Acme Broomcorn, BTx3197, P850029, SC500, 90M, SC1439, SC301, and P898012. These genotypes were selected based on their i) seed availability, ii) height (< 3m to accommodate imaging hardware) and iii) high/low kinship values within each of nine SAP subpopulations (Casa et al., 2008).

The experiment was conducted from June 11 to September 20, 2019, in the greenhouse at the University of Nebraska-Lincoln's Greenhouse Innovation Center. Sorghum seeds were planted in 1.5-gallon pots filled with a soil mixture of two-thirds peat moss, one-third vermiculite, and 2,187 g/m³ lime. Pots were weighed and watered to saturation with a 100 ppm calcium chelate solution (Miller Chemical & Fertilizer, LLC, Hannover, PA, USA). From June 14 (3 days after planting, DAP) to June 23, 2019 (12 DAP), a 20-10-20 NPK fertilizer was applied daily in liquid form until saturation to ensure seedling survival. Seedling emergence occurred on June 16, 2019 (5 DAP).

The experimental setup of the sorghum plants used in this study is illustrated in Fig. 1A. Two sets of sorghum plants were grown: one for imaging-based phenotyping and the other for destructive RNA-Seq sampling. The phenotyping set comprised 110 sorghum plants, divided into two groups. The first group is the Tx430 group, consisting of 20 Tx430 plants that are split into four treatment units (five plants per unit as replicates). Each unit received one of four nitrogen fertilizer treatments (6, 9, 12, or 15 mM nitrogen) applied as 250 mL of Hoagland solution twice weekly, starting at 27 DAP until harvest. The Hoagland solution composition, with nitrogen supplied as potassium nitrate (KNO_3) and calcium nitrate ($Ca(NO_3)_2 \cdot 4H_2O$), is detailed in Table S1. The second group is the SAP group consisting of 90 plants from nine diverse SAP lines, divided into two treatment units (45 plants each, with five replicates per line), each receiving either 6 mM or 12 mM nitrogen treatments (N treatments).

The RNA-Seq sampling set consisted of 48 Tx430 plants grown off the phenotyping belt in the same greenhouse. These were divided into four experimental units (12 plants per unit), each

receiving one of the four N treatments (6, 9, 12, or 15 mM). Destructive RNA sampling was conducted at four developmental stages: vegetative, boot, anthesis, and grain fill. At each stage, the leaf attached to node five from the bottom was sampled from three biological replicates, immediately flash-frozen in liquid nitrogen, and stored for RNA isolation.

Imaging based phenotyping

Sorghum plants were phenotyped using a LemnaTec Scanalyzer 3D high-throughput plant phenotyping system (LemnaTec GmbH, Aachen, Germany). Starting on July 13, 2019 (32 days after planting, DAP) and continuing through September 19, 2019 (100 DAP), pots containing individual sorghum plants were placed on an automated conveyor belt system for scheduled imaging. Each plant was imaged individually across four sensor modalities: visible-near infrared (VNIR) hyperspectral imaging, thermal infrared, steady-state chlorophyll fluorescence, and RGB (visible) imaging, as described in Ge et al. (2016) and Miao et al. (2020). Grayscale hyperspectral images in the VNIR spectrum were acquired with a Headwall Hyperspec Ext-VNIR camera (Headwall Photonics, Bolton, MA, USA). High-resolution RGB images were captured using a Prosilica GT6600 camera (Allied Vision Technology, Stadtroda, Germany) at 4384 x 6576 pixels (horizontal x vertical).

Manual pixel annotation

A single hyperspectral data cube in this study is a collection of 243 grayscale image files in PNG format obtained from imaging of one plant at a single time point, with each image representing light intensity at a different wavelength between 546 to 1700 nm at 4.77 nm intervals. We classified the pixels into six different pixel classes, green leaf, yellow leaf, dry leaf, stalk, panicle, and background. Plant tissues were segmented into five different parts: green leaf, yellow leaf, dry leaf, stalk, and panicle.

As no single wavelength can distinguish all six pixel classes, we used human annotators to assign ground truth category labels to each of the six pixel classes to train the machine learning algorithm. A total of 74 hyperspectral images taken on the last day of imaging at 100 DAP (Table S2) were used to generate the ground truth category labels. These images spanned different sorghum genotypes and N treatments used in the experiments. Human annotators were provided two types of images, one image representing a specific wavelength within the hyperspectral datacube (image 187, corresponding to light intensity at 1,434 nm), and a paired RGB image of the same plant. These images were used together for annotation purposes by mirroring the RGB image along the y-axis and merging the two images together. From our observation, the image at 1,434 nm wavelength provided the best contrast between plant tissue and image background. Human annotators worked through Zooniverse (https://www.zooniverse.org/projects/alejandropages/sorghum-and-maize-segmentation-using-hyperspectral-imagery) to mark the position of six different pixel classes on the grayscale hyperspectral image - green leaf, yellow leaf, dry leaf, stalk, panicle, and background - using the RGB image as a reference. From each plant image we collected up to ten pixels per class for further model training and evaluation.

For each ground truth labeled pixel in the hypercube, we extracted the intensity values from pixels at the same position in each of the 243 images representing the 243 wavelengths as measured by the hyperspectral camera. These produced a vector of 243 intensity values for each ground truth labeled pixel that were used as the input to train machine learning classifiers to classify each pixel in the hyperspectral cube collected into one of the six different pixel classes.

Model training and model evaluation

Machine learning models were used to classify each pixel in the hyperspectral cube into one of the six different pixel classes, green leaf, yellow leaf, dry leaf, stalk, panicle, and background. We evaluated four different machine learning models: a support vector machine with radial basis function kernel and class weights (SVM) (Karatzoglou et al., 2004), elastic net regularization regression (Glmnet) (Friedman et al., 2010), partial least squares discriminant analysis (PLS-DA) (Mevik et al., 2020; Mevik & Wehrens, 2007), and linear discriminant analysis (LDA) (Venables & Ripley, 2002). These methods were evaluated using a five-fold cross validation. Due to the imbalance between the number of pixel data points among the six different pixel classes, we performed an upsampling step prior to randomly sub-sampling the data to generate training and testing dataset for k-fold cross validation. All model evaluations for pixel classification and image segmentation were performed using the caret and caretEnsemble package in R version 4.0.3 (Deane-Mayer & Knowles, 2019; Kuhn, 2020).

Hyperspectral image pixel classification

Classification of each pixel within the hypercube dataset into the six different pixel classes was performed using methods described in Miao et al. (2020) with modification to allow for additional pixel classification for yellow leaf and dry leaf. Whole image classification was performed on a subset of the imaging data collected by the automated phenotyping system, encompassing only images from Tx430 plants taken between July 13, 2019 (32 DAP) to September 19, 2019 (100 DAP). This subset of 672 hyperspectral images was further subjected to pixel classification to obtain pixel counts for each of the six different pixel classes.

We performed calculations to convert pixel counts from the five different pixel categories representing sorghum plant tissues into their respective areas. To do this, we used the top diameter of the pots within each image as a useful internal measure or 'scale' to convert pixel coverage into area in cm^2. In simple terms, we first calculated the length (in cm) spanned by each pixel by dividing the top diameter of the pot (21.59 cm) with the number of pixels spanning the top diameter of the pot in each hypercube image. Since pixels are square shaped, we squared this length to obtain the area each pixel represented in cm^2. When multiplied by the number of pixels from each of the five pixel classes, we could obtain the total area covered by each of those pixel categories. Mathematically, this would be equal to scaling the pixel counts at each pixel class by multiplying it with a correction factor and converting it into area in cm^2 (Eq. 1).

Prior to whole image classification, areas within the image corresponding to the pot and background structure were cropped out from the image to enable a more accurate pixel count for each of the pixel classes. Due to the growth of the plants, images taken at an earlier growth stage were at a higher magnification than images taken at a later growth stage. Both the cropping and the conversion of pixel counts into areas accounted for the different magnification levels between hyperspectral cube images of the same plants.

$$Total\ area\ in\ cm^2 = \left(\frac{21.59}{pot\ top\ diameter\ pixel\ count}\right)^2 \times pixel\ count \quad \textbf{(Equation 1)}$$

Senescence ratio was calculated after converting each pixel class count to surface area. The senescence ratio was defined as the sum of yellow and dry leaf area divided by green leaf area (Eq. 2).

$$Senescence\ ratio = \frac{yellow\ leaves\ area + dry\ leaves\ pixel\ area}{green\ leaves\ area} \quad \textbf{(Equation 2)}$$

RNA extraction and RNA-Seq

Sorghum leaf tissue was ground to fine powder using Freezer/Mill® (Cole-Palmer, NJ, USA) and stored at -80 °C. RNA was extracted using the CTAB method (Chang et al., 1993) with the following modification. MaXtract High Density tubes (Qiagen, Germantown, MD, USA, cat. no. 129065) were used for the phenol:chloroform organic extraction step as per the manufacturer's instructions. RNA concentration was determined using NanoDrop One^c (Thermo Scientific). 10 µg of DNase (Thermo Scientific TURBO™ DNase, AM2239) treated RNA was column purified using Zymo Direct-Zol-96 RNA kit (R2056). A final quality and quantity assessment was done on 2100 Agilent Bioanalyzer using RNA 6000 Nano Kit (5067-1511, Agilent) and SpectraMax iD3 (Molecular Devices) plate reader using Quant-iT RNA assay kit (Q10213, ThermoFisher Scientific) and sequenced on an Illumina NovaSeq 6000 and deposited on NCBI's Short Read Archive (BioProject PRJNA1452908, SRR38119224 to SRR38119282)

150 bp paired-end strand-specific RNA-Seq reads were processed to remove adapters and low-quality bases (Q<25) with custom Python scripts. Reads that were shorter than 50 bp post-trimming were discarded. The resulting high-quality reads were aligned to the *Sorghum bicolor* 'RTx430' reference genome v2.1 (Cole et al., 2026) using the short-read alignment tool, GSNAP (version 2023-10-10 Wu & Nacu, 2010) and read counts for annotated genes were generated using HTSeq v1.99.2 (Anders et al., 2015). The biological replicates were used to identify outliers, which were then removed based on the Euclidean distance from the cluster center and a Pearson correlation coefficient ($r \geq 0.85$). Libraries passing this quality control and outlier filtering were used for downstream analysis. Gene expression was quantified as the number of fragments per kilobase of exon per million mapped fragments (FPKM) and transcripts per million (TPM), calculated by normalizing read counts to gene length and total mapped reads per sample (B. Li & Dewey, 2011; Trapnell et al., 2011). We required ≥2 normalized relative log expression counts per gene in at least two samples for them to remain in the analysis.

Gene expression correlation with senescence and construction of gene regulatory networks

To evaluate the impact of soil nitrogen level on sorghum development, we analyzed the transcriptional profiles of the fifth nodal leaf (counted from the bottom) from Tx430 plants sampled across four developmental stages and four nitrogen levels, alongside their corresponding senescence ratios (Eq. 2). There were 3 biological replicates per collection. Gene expression values (TPM) were correlated with the senescence ratio within each growth stage, N treatment, and across the developmental timeline. The top 100 genes showing the strongest positive correlation with the senescence ratio (Pearson correlation coefficient, $r \geq 0.85$) were identified and subjected to Gene Ontology (GO) enrichment analysis to assess their biological relevance to senescence. Predicted transcription factors (TFs) among these genes were further evaluated for previously reported biological functions using PaperBLAST (Price & Arkin, 2017). Gene regulatory networks (GRNs) were then constructed for TFs with strong associations to senescence using GENIE3 (Huynh-Thu et al., 2010), and the top 1% of regulatory connections were analyzed for GO enrichment to infer biological processes.

GO enrichment analysis

GO Ontology and annotations obtained from InterPro to GO mappings (v53.0) were used for GO enrichment analysis of differentially expressed genes (DEGs) using topGO (v.2.42.0) (Alexa A and Rahnenfuhrer J, 2016), an R Bioconductor package, to determine overrepresented GO categories across biological process (BP), cellular component (CC), and molecular function (MF) domains. Enrichment of GO terms was tested using Fisher's exact test with $P < 0.05$ considered significant.

Results

Performance of machine learning algorithms in pixel classification

Four different machine learning algorithms were evaluated on their ability to classify the pixels in a hypercube image into six classes: green leaf, yellow leaf, dry leaf, stalk, panicle, and background (see Material and Methods). The training dataset, comprising 8,787 manually annotated pixels, was curated through crowdsourcing on the Zooniverse platform. Each pixel was labeled into one of the six defined classes (Fig. 1B and Table S3). Notably, the number of pixels representing the panicle class was relatively low due to delayed flowering and/or the small panicle size, reflecting natural variation in the ground truth dataset (Table S3). Among the algorithms, LDA and PLS-DA achieved the lowest accuracy of 0.91, followed by Glmnet at 0.92. SVM delivered the highest accuracy of 0.93 (Fig. 1C). Consequently, SVM was selected for

further pixel classification in the hyperspectral cube. Despite the high overall accuracy of the SVM model, a small fraction of pixels was misclassified as panicle tissue, even in images of young sorghum plants. These misclassified pixels were primarily located along the leaf midrib and edges (Fig. S1). Nonetheless, the pixel-wise segmentation into plant tissue classes was effective and enabled the identification of leaf senescence patterns.

Hyperspectral signatures of sorghum under varying nitrogen levels

The average hyperspectral spectral intensity profiles from the pixel training data for green leaf, yellow leaf, dry leaf, stalk, panicle, and background pixel classes were calculated and visualized (Fig. 1D). Green-leaf and yellow-leaf classes exhibited distinct spectral intensities in the visible spectrum, particularly below 700 nm, corresponding to the red region (600–700 nm). This divergence likely reflects differences in chlorophyll content and leaf senescence. In the near-infrared (NIR, 750–1400 nm) spectrum, all pixel classes displayed unique spectral intensity patterns, with notable variations in intensity driven by differences in tissue structure and water content. The dry leaf class showed a pronounced divergence from other classes starting at approximately 1350 nm, near the NIR boundary, and extending into the short-wave infrared (SWIR, 1400–3000 nm) spectrum at around 1700 nm. This pattern is consistent with reduced water absorption and altered cellular structure in senescent tissue, distinguishing dry leaves from other plant tissues (Fig. 1D).

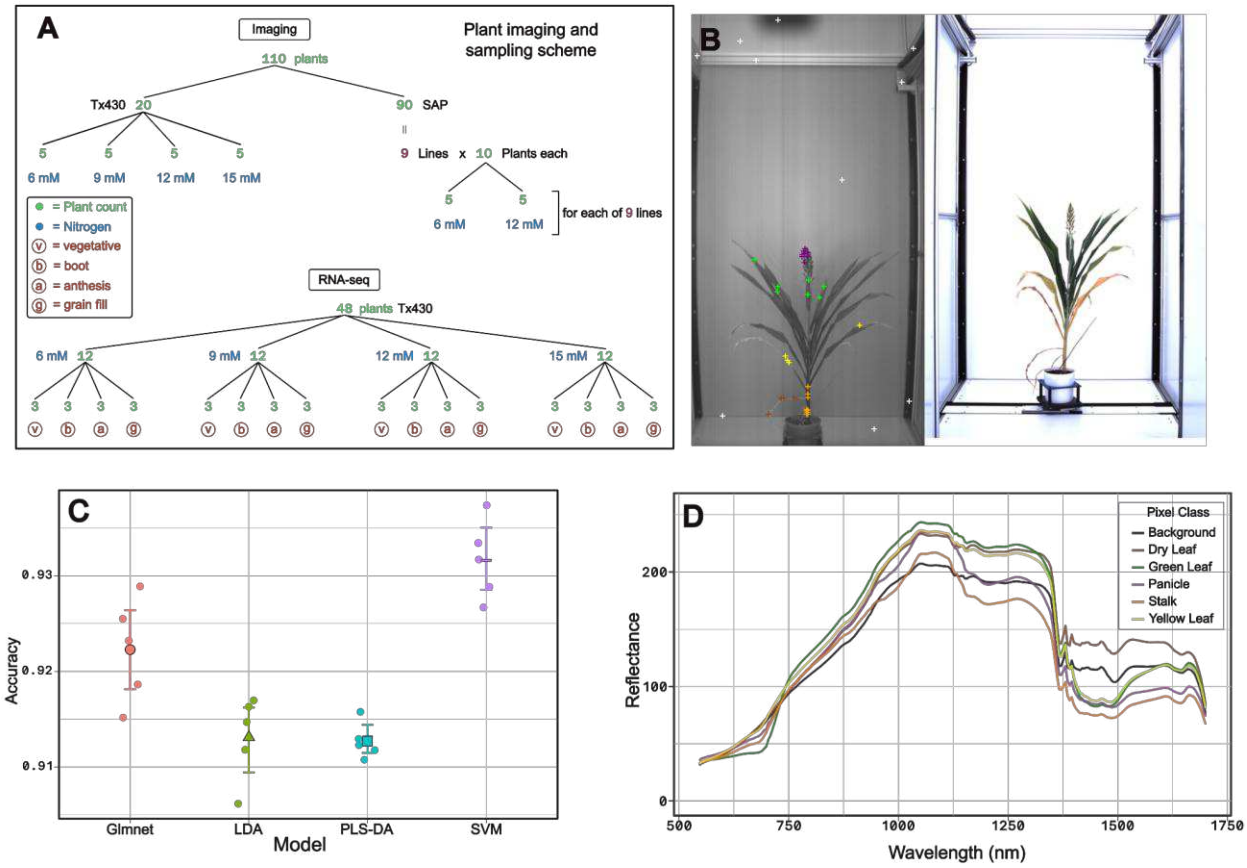

Figure 1. Identifying hyperspectral signatures of sorghum tissue types. (A) Experimental design of the sorghum plants used for data collection. (B) Manual pixel annotation of a sorghum hyperspectral image. The right side is the RGB image of a sorghum plant and the left side is its hyperspectral image. In the left image, the '+' signs are six pixel categories manually annotated based on the RGB image. Except for the background pixel +s which are white, the color coding for tissues are the same as in 1D. (C) Performance of four machine learning methods in classifying pixels. Model training was done with five-fold cross validation. Error bars represent 95% confidence intervals. (D) Average spectral intensity pattern (546-1700 nm) of the six pixel classes (background, dry leaf, green leaf, stalk, panicle, and yellow leaf) from the training dataset. Distinct patterns in the visible (550–700 nm), near-infrared (NIR, 750–1400 nm), and short-wave infrared (SWIR, 1400–3000 nm) spectra reflect tissue-specific composition and senescence.

Soil nitrogen enhances growth and yield in Sorghum 'Tx430'

Using SVM classification, we distinguished tissues of *S. bicolor* 'Tx430' (green leaf, yellow leaf, dry leaf, stalk, panicle) across hyperspectral images (Fig. 2A and Fig. S1). Pixel area counts for

these five tissue types served as a proxy for biomass distribution across developmental stages. The total biomass increased with the amount of applied N (Fig. 2A and 2B).

Green leaf pixel counts exhibited a consistent increase, peaking at the reproductive/boot stage (76–86 DAP, varying by treatment), followed by a decline as sorghum transitioned to reproductive growth across all N levels (Fig. 2A). This reliable pattern served as an effective proxy for green leaf biomass, with nitrogen availability modulating the timing and magnitude of peak biomass accumulation. Up to 75 DAP, the proportion of dry leaf area was similar for all N treatments. After that, plants under low N (6 mM) exhibited a higher proportion of dry leaf area, reflecting accelerated senescence, whereas those under high N (15 mM) showed the lowest proportion of these pixel classes, consistent with enhanced leaf vitality (Fig. S2B). Plants with low N showed a higher proportion of yellow leaf areas compared to high N treatment up to 95 DAP. After that, there was an increase in yellow leaf areas in the high N treatments compared to the low N treatments (Fig. S2C).

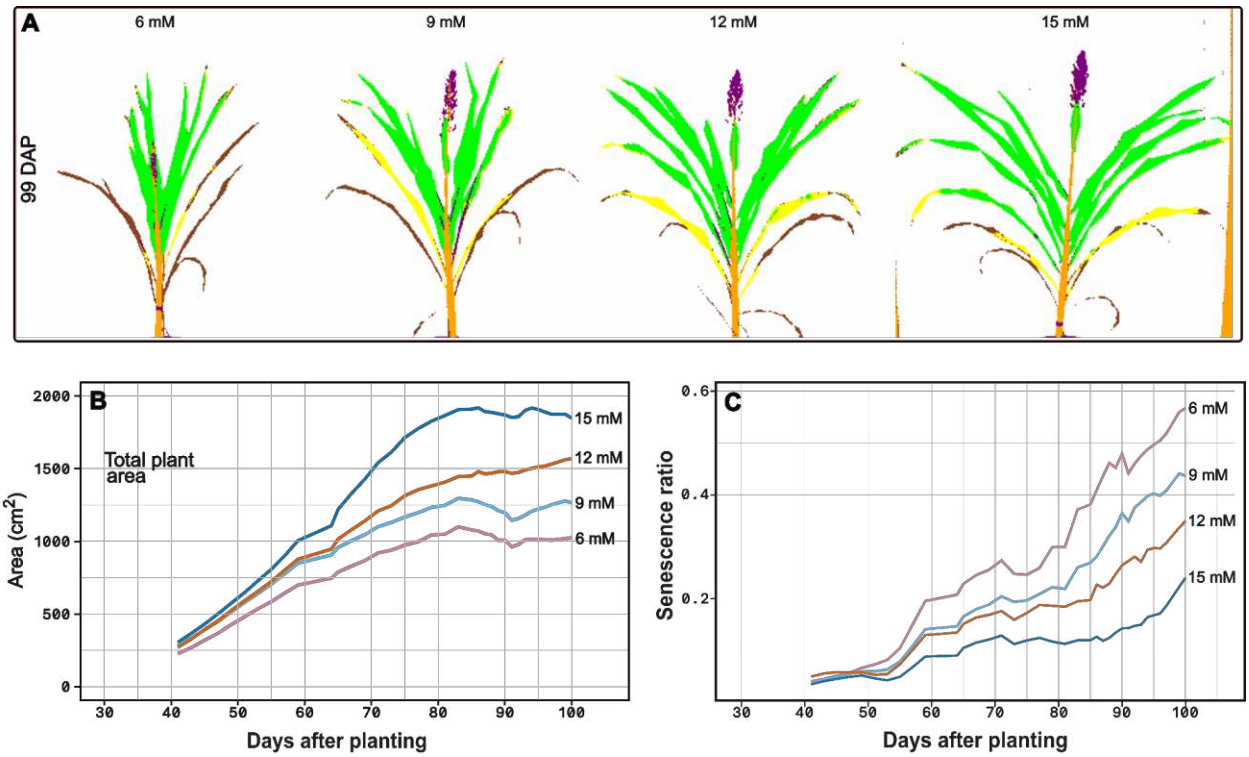

Figure 2. Sorghum Tx430 growth and senescence under varying nitrogen treatments (6, 9, 12 and 15mM). (A) Tissues segmented by the SVM model (segmentation classes: green leaf (green), yellow leaf (yellow), dried leaf (brown), stalk (orange), panicle (purple) and background (white)) at 99 days after planting. (B) Total tissue area and (C) Senescence ratio. Measurements were derived from hyperspectral images collected from the vegetative to grain fill stages and a moving average calculated across seven consecutive measurements.

To quantify the effect of nitrogen limitation on senescence, we calculated the senescence ratio (Eq. 2) and plotted it over time (Fig. 2C). From 55 to 100 DAP, higher N levels (12 and 15 mM) corresponded to lower senescence ratios, indicating delayed senescence under higher N. Overall, all treatments showed a gradual, parallel increase in senescence ratio (Fig. 2C). This consistent rise in senescence ratio across developmental stages mirrors the dynamics of sorghum growth and senescence, with nitrogen sufficiency delaying senescence.

Nitrogen limitation triggers leaf senescence transcriptional response

We then looked at how these senescence ratio patterns change across growth stages (vegetative, boot, anthesis, & grain fill) under varying N treatments (6, 9, 12, and 15 mM). Senescence ratio remained relatively consistent during the vegetative stage across N levels. However, at the boot, anthesis, and grain-fill stages, senescence ratio consistently decreased with increasing N concentrations (Fig. 3A).

To investigate the relationship between nitrogen availability, senescence, and gene expression, we analyzed transcriptional profiles from the leaf at the fifth node of Tx430 across four growth stages and four N levels and paired these data with senescence ratio. The fifth nodal leaf was selected because it was consistently present across images and showed variation in senescence status. By integrating pixel-based senescence data with transcriptional profiles, we identified genes positively correlated with senescence ratio across N treatments for each developmental stage (Supplementary Data file 1 shows the top 100 genes) and across the developmental timeline (Supplementary Data file 2). Among these genes, 13 were annotated as TFs, including two WRKY TFs: SbiRTX430.02G247100 (homolog of Arabidopsis WRKY1/ZAP1, AT2G04880, zinc-dependent Activator Protein 1) and SbiRTX430.07G116400 (homolog of Arabidopsis WRKY4, AT1G13960). Gene regulatory networks were constructed for these TFs, and the top 1% of connections were assessed for GO enrichment (Fig. 3C). For SbiRTX430.02G247100 (WRKY1/ZAP1), GO terms related to positive regulation of leaf senescence and chlorophyll catabolism were significantly enriched (Fig. 3D). For SbiRTX430.07G116400 (WRKY4), positive regulation of autophagosome assembly, a process associated with senescence and nitrogen remobilization, ranked among the top 10 enriched GO terms (Fig. S3). These results identify candidate genetic components associated with N-limitation-induced senescence in Tx430 and demonstrate the utility of combining transcriptional and phenotypic data for hypothesis generation.

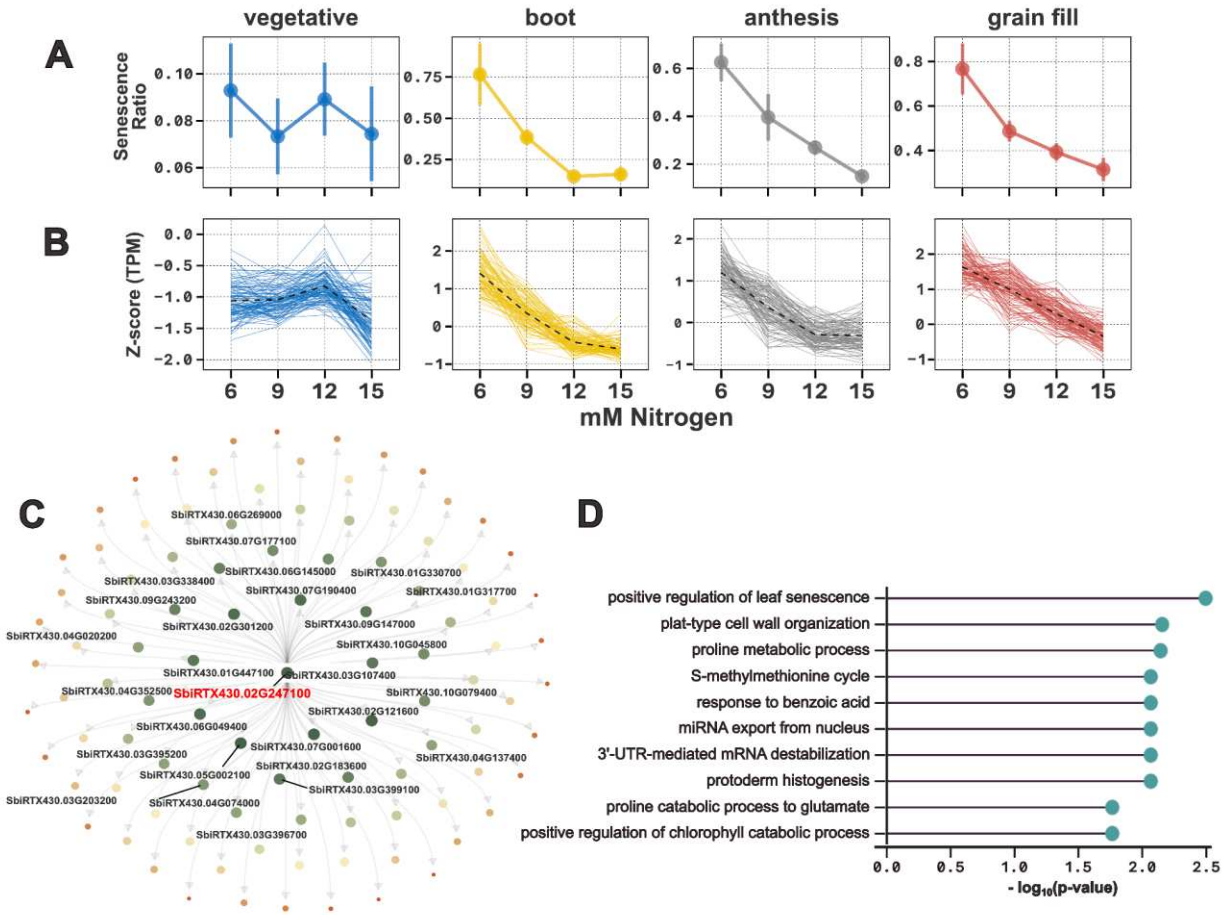

Figure 3. Correlation between leaf senescence, computed through image analysis, and gene expression under different levels of soil N. (A) Senescence ratio across the four growth stages under varying nitrogen (N) treatment levels. Error bars represent standard deviation. (B) RNA expression profiles of the top 100 genes that are positively correlated (Pearson Correlation Coefficient, r ≥ 0.85) with senescence ratio measured across four developmental stages and N treatments. Z-score normalized TPM (Transcripts Per Million) values were plotted to visualize gene expression patterns. (C) Gene regulatory network of SbiRTX430.02G247100, a senescence-associated transcription factor identified among these top 100 genes. (D) Enriched Gene Ontology (GO) terms among genes in the regulatory network from panel (C). NOTE: In (A) and (B), the scale of Y-axes differ among the 4 stages.

Discussion

Manual phenotyping of plant traits, such as senescence, is labor-intensive and low-throughput, limiting the scale and scope of studies (Miao et al., 2020). Traditional methods like visual inspection or SPAD measurements are particularly challenging for senescence due to its dynamic nature, requiring high temporal and potentially spatial resolution to capture variability in onset and progression (Chapman et al., 2021; Wingler et al., 2004). This study addresses these

challenges by implementing high-throughput hyperspectral imaging (HSI) coupled with machine learning to quantify senescence in sorghum (Tx430) across four growth stages (vegetative, boot, anthesis, and grain fill) under varying N levels (6, 9, 12, and 15 mM). This approach enabled precise tracking of senescence dynamics and identified candidate molecular components associated with nitrogen-limitation-induced senescence.

We employed HSI-based methods, utilizing 243 wavelengths (546–1700 nm) and machine learning, to successfully segment sorghum tissues into five classes (green leaf, yellow leaf, dry leaf, stalk, and panicle). Among the four machine learning models evaluated, SVM classifier outperformed Glmnet, PLS-DA, and LDA, achieving the highest classification accuracy (0.93) (Fig. 1C). This contrasts with previous work in sorghum where LDA was reported to be the most effective classifier for simpler tissue segmentation tasks (Miao et al., 2020). Our findings suggest that SVM is more robust when classifying multiple, closely related tissue types, especially under varying N conditions.

Despite high overall accuracy (Fig. 1C), our HSI analysis revealed certain limitations. For example, dry leaf pixel counts exhibited significant temporal fluctuations, likely due to erroneous classification because they tend to wrinkle when they dry. Similarly, panicle pixels were detected before panicle emergence, primarily along leaf midribs and edges. This error aligns with prior studies reporting spectral overlap between lignified tissues, that leads to leaf midribs being misclassified as stalk or panicle in sorghum (Miao et al., 2020). Another limitation is the inherent unbalance in the training data set that we addressed by up-sampling the training dataset to reduce false positives and increasing accuracy (Tran et al., 2022), enabling reliable differentiation of green, yellow, and dry leaf classes and accurate senescence ratio estimation. Nonetheless, refining spectral signatures or adopting advanced approaches, such as hybrid machine learning models, could further improve tissue classification precision.

When we tracked the yellow leaf areas among the N treatments, after 95 DAP, there was a reversal in yellow leaf area among the high N treatments vs. the low N (Fig. S2C). It increased in the high N treatments after having trailed for most of the life of the plant. This could be due to the quick senescing of higher area of green leaves in the high N, driving up the yellow leaf area. Since the experiment was stopped at day 100, these yellow leaves might not have dried quickly enough to be detected in the dry leaf category.

The senescence ratio effectively tracked senescence progression across growth stages and N treatments. During the vegetative stage, we observed minimal differences in senescence ratio among N treatments, consistent with limited senescence-associated remobilization at this stage. This is consistent with findings in Arabidopsis, where nitrogen deficiency does not strongly induce senescence during vegetative growth (Diaz et al., 2008). In contrast, higher senescence ratios at lower N levels during boot, anthesis, and grain-fill stages suggest an adaptive response to nitrogen limitation by enhancing remobilization. This aligns with the study linking nitrogen deficiency to accelerated senescence for nutrient reallocation (Hawkesford & Griffiths, 2019).

To explore the molecular basis of nitrogen-responsive senescence, we integrated gene expression profiles with senescence ratio measurements. Transcriptomics on the fifth nodal leaf

across the four growth stages revealed genes whose expression was positively correlated with the senescence ratio. Notably, 13 of the top 100 genes were TFs, including two WRKY family members, SbiRTX430.02G247100 (homologous to Arabidopsis *WRKY1/ZAP1*) and SbiRTX430.07G116400 (homologous to *WRKY4*). *WRKY1/ZAP1* (AT2G04880) has been implicated in multiple regulatory pathways involving stress responses (Edrisi Maryan et al., 2023; Qiao et al., 2016), salicylic acid (SA) signaling, flowering, and nitrogen remobilization (W. Zhang et al., 2024). Overexpression of *WRKY1/ZAP1* in Arabidopsis accelerates both flowering and senescence, while mutants show delayed developmental progression (W. Zhang et al., 2024), highlighting its role in coordinating life cycle transitions. *WRKY4*, on the other hand, is responsive to SA, salt, and methyl jasmonate stresses and is expressed early during senescence (Breeze et al., 2011; Buchanan-Wollaston et al., 2005; Datta et al., 2013; P. Li et al., 2021; Wagstaff et al., 2009) . Gene regulatory network analysis revealed that genes co-expressed with *WRKY1/ZAP1* were enriched for GO terms related to leaf senescence, cell wall organization, and proline metabolism. This enrichment suggests a functional role in orchestrating physiological responses during senescence. *WRKY4*'s network was enriched for terms associated with photoperiodism, autophagy, and stomatal regulation, pointing to its potential involvement in regulating stress-induced senescence and developmental timing.

Proline catabolic processes were enriched among *WRKY1/ZAP1*-associated genes. Proline catabolism is associated with ATP production in senescing petals, but in leaves it may have additional roles in nitrogen recycling through glutamate metabolism or in hormone signaling pathways (Masclaux-Daubresse et al., 2005; L. Zhang & Becker, 2015). These results suggest that WRKY1/ZAP1 may be part of a regulatory module linking stress and hormone signaling with senescence progression and NUE.

Conclusions

By integrating high-throughput hyperspectral phenotyping with transcriptomic analysis we identified transcription factor networks associated with nitrogen-responsive senescence in sorghum. The senescence patterns we observed under nitrogen limitation are consistent with enhanced remobilization of internal nitrogen reserves, although direct measurements of nitrogen flux will be needed to test this relationship explicitly. The WRKY1/ZAP1- and WRKY4-associated gene networks identified here provide candidate regulatory modules for future functional studies, particularly in relation to phytohormone signaling, senescence progression, and NUE-associated traits. Extending this framework to genetically diverse sorghum panels could reveal patterns of natural variation in senescence dynamics and nitrogen remobilization-associated traits relevant to breeding for improved NUE. We believe that HSI-based phenotyping can complement association mapping (Bollam et al. 2026), transcriptomic (Braynen et al. 2025; Gu et al. 2025), and metabolomic (Gu et al. 2025) analyses, to dissect the molecular mechanisms underlying any dynamic stress-responsive trait and support efforts to develop varieties that are more resilient and better suited to a variety of environments.

518

List of abbreviations

N: Nitrogen

NUE: Nitrogen Use Efficiency

GO: Gene Ontology

GRN: Gene Regulatory Network

SPAD: Soil Plant Analysis Development

NIR: Near-Infrared

VNIR: Visible-Near Infrared

RGB: Red Green Blue (Visible Light)

PNG: Portable Network Graphics

SVM: Support Vector Machine

PLS-DA: Partial Least Squares Discriminant Analysis

LDA: Inear Discriminant Analysis

TPM: Transcripts Per Million

TF: Transcription Factor

BLAST: Basic Local Alignment Search Tool

DEG: Differentially Expressed Genes

BP: Biological Process

CC: Cellular Component

MF: Molecular Function

SWIR: Short-Wave Infrared

DAP: Days After Planting

HSI: Hyper Spectral Imaging

SAP: Sorghum Association Panel

FPKM: Fragments Per Kilobase of exon per Million mapped fragments

GB: GigaBytes

Declarations

Ethics approval and consent to participate

Not applicable

Consent for publication

Not applicable

Availability of data and materials

The datasets generated during the current study are available in the NCBI SRA repository, under BioProject PRJNA1452908 (https://www.ncbi.nlm.nih.gov/bioproject/PRJNA1452908) (RNA-seq raw reads SRR38119224 to SRR38119282). Scripts used for image processing, machine-learning classification, transcriptomic analyses, and figure generation will be accessible through GitHub (https://github.com/belafif2/TX430_Senescence). Image data (148 GB) will be made available in a data repository upon acceptance. Other relevant processed data files and supporting figures are available as supplementary data documents.

Competing interests

The authors declare that they have no competing interests.

Funding

This work was funded by NSF EPSCoR Track-2 Award Number 1826781, U.S. Department of Energy, Office of Science, Biological and Environmental Research Program under Award Number DE-SC0023138 and the DOE Center for Advanced Bioenergy and Bioproducts Innovation (U.S. Department of Energy, Office of Science, Biological and Environmental Research Program under Award Number DE-SC0018420). Any opinions, findings, and conclusions or recommendations expressed in this publication are those of the author(s) and do not necessarily reflect the views of the National Science Foundation or the U.S. Department of Energy.

Authors' contributions

AS, JS, JCS, and KS designed the experiment.

MZ and SM performed the experiment and collected samples.

PH, and MG mentored the graduate and high school students who did the analysis.

SMyler and BD performed image annotation on zooninverse for model training.

MG wrote the initial scripts for image analysis.

MZ, MG, and MBB analyzed the image data.

AS analyzed the transcriptomic data and worked with MBB to integrate it with the image data.

ZJ compiled the image data.

GB made all the figures and charts and assembled them into panels for visualization.

MBB, MZ, and AS wrote the original draft of the manuscript.

MBB, AS, GB, YG, JG, JS, JCS, and KS reviewed and edited the draft manuscript.

JS, JCS, and KS provided funding for the experiment and data analysis.

Acknowledgements

We'd like to thank the greenhouse staff at the University of Nebraska Lincoln for help with the plants, and the Schnable lab for help with tissue sampling. We would also like to thank the high school and summer interns, and George R. Berry, for their help with manual annotation of images on Zooniverse.

References

Anderegg, J., Yu, K., Aasen, H., Walter, A., Liebisch, F., & Hund, A. (2019). Spectral Vegetation Indices to Track Senescence Dynamics in Diverse Wheat Germplasm. *Frontiers in Plant Science*, *10*, 1749. https://doi.org/10.3389/fpls.2019.01749

Anders, S., Pyl, P. T., & Huber, W. (2015). HTSeq-A Python framework to work with high-throughput sequencing data. *Bioinformatics* , *31*(2), 166–169. https://doi.org/10.1093/bioinformatics/btu638

Baloch, F. S., Altaf, M. T., Liaqat, W., Bedir, M., Nadeem, M. A., Cömertpay, G., Çoban, N., Habyarimana, E., Barutçular, C., Cerit, I., Ludidi, N., Karaköy, T., Aasim, M., Chung, Y. S., Nawaz, M. A., Hatipoğlu, R., Kökten, K., & Sun, H.-J. (2023). Recent advancements in the breeding of sorghum crop: current status and future strategies for marker-assisted breeding. *Frontiers in Genetics*, *14*, 1150616. https://doi.org/10.3389/fgene.2023.1150616

Barneix, A. J. (2007). Physiology and biochemistry of source-regulated protein accumulation in the wheat grain. *Journal of Plant Physiology*, *164*(5), 581–590. https://doi.org/10.1016/j.jplph.2006.03.009

Boatwright, J. L., Sapkota, S., Jin, H., Schnable, J. C., Brenton, Z., Boyles, R., & Kresovich, S. (2022). Sorghum Association Panel whole-genome sequencing establishes cornerstone resource for dissecting genomic diversity. *The Plant Journal : For Cell and Molecular Biology*, *111*(3), 888–904. https://doi.org/10.1111/tpj.15853

Breeze, E., Harrison, E., McHattie, S., Hughes, L., Hickman, R., Hill, C., Kiddle, S., Kim, Y.-S., Penfold, C. A., Jenkins, D., Zhang, C., Morris, K., Jenner, C., Jackson, S., Thomas, B., Tabrett, A., Legaie, R., Moore, J. D., Wild, D. L., … Buchanan-Wollaston, V. (2011). High-resolution temporal profiling of transcripts during Arabidopsis leaf senescence reveals a distinct chronology of processes and regulation. *The Plant Cell*, *23*(3), 873–894.

https://doi.org/10.1105/tpc.111.083345

Buchanan-Wollaston, V., Page, T., Harrison, E., Breeze, E., Lim, P. O., Nam, H. G., Lin, J.-F., Wu, S.-H., Swidzinski, J., Ishizaki, K., & Leaver, C. J. (2005). Comparative transcriptome analysis reveals significant differences in gene expression and signalling pathways between developmental and dark/starvation-induced senescence in Arabidopsis. *The Plant Journal: For Cell and Molecular Biology*, *42*(4), 567–585. https://doi.org/10.1111/j.1365-313X.2005.02399.x

Cai, J., Okamoto, M., Atieno, J., Sutton, T., Li, Y., & Miklavcic, S. J. (2016). Quantifying the Onset and Progression of Plant Senescence by Color Image Analysis for High Throughput Applications. *PloS One*, *11*(6), e0157102. https://doi.org/10.1371/journal.pone.0157102

Casa, A. M., Pressoir, G., Brown, P. J., Mitchell, S. E., Rooney, W. L., Tuinstra, M. R., Franks, C. D., & Kresovich, S. (2008). Community Resources and Strategies for Association Mapping in Sorghum. *Crop Science*, *48*(1), 30–40. https://doi.org/10.2135/cropsci2007.02.0080

Chang, S., Puryear, J., & Cairney, J. (1993). A simple and efficient method for isolating RNA from pine trees. *Plant Molecular Biology Reporter*, *11*(2), 113–116. https://doi.org/10.1007/BF02670468

Chapman, E. A., Orford, S., Lage, J., & Griffiths, S. (2021). Capturing and Selecting Senescence Variation in Wheat. *Frontiers in Plant Science*, *12*, 638738. https://doi.org/10.3389/fpls.2021.638738

Chen, K.-E., Chen, H.-Y., Tseng, C.-S., & Tsay, Y.-F. (2020). Improving nitrogen use efficiency by manipulating nitrate remobilization in plants. *Nature Plants*, *6*(9), 1126–1135. https://doi.org/10.1038/s41477-020-00758-0

Cole, B., Zhang, W., Shi, J., Wang, H., Baker, C., Varoquaux, N., Hollingsworth, J., Hutmacher, R., Dahlberg, J., Pierroz, G., Barry, K. W., Singan, V., Yoshinaga, Y., Daum, C., Zane, M., Blow, M., O'Malley, R., Shu, S., Jenkins, J. W., … Vogel, J. P. (2026). Multi-

season analysis reveals hundreds of drought-responsive genes in sorghum. *The Plant Journal: For Cell and Molecular Biology*, *125*(3), e70657. https://doi.org/10.1111/tpj.70657

Congreves, K. A., Otchere, O., Ferland, D., Farzadfar, S., Williams, S., & Arcand, M. M. (2021). Nitrogen Use Efficiency Definitions of Today and Tomorrow. *Frontiers in Plant Science*, *12*, 637108. https://doi.org/10.3389/fpls.2021.637108

Datta, R., Sinha, R., & Chattopadhyay, S. (2013). Changes in leaf proteome profile of Arabidopsis thaliana in response to salicylic acid. *Journal of Biosciences*, *38*(2), 317–328. https://doi.org/10.1007/s12038-013-9308-9

Deane-Mayer, Z. A., & Knowles, J. E. (2019). *caretEnsemble: Ensembles of Caret Models*. https://CRAN.R-project.org/package=caretEnsemble

Deschamps, S., Zhang, Y., Llaca, V., Ye, L., Sanyal, A., King, M., May, G., & Lin, H. (2018). A chromosome-scale assembly of the sorghum genome using nanopore sequencing and optical mapping. *Nature Communications*, *9*(1), 4844. https://doi.org/10.1038/s41467-018-07271-1

Diaz, C., Lemaître, T., Christ, A., Azzopardi, M., Kato, Y., Sato, F., Morot-Gaudry, J.-F., Le Dily, F., & Masclaux-Daubresse, C. (2008). Nitrogen recycling and remobilization are differentially controlled by leaf senescence and development stage in Arabidopsis under low nitrogen nutrition. *Plant Physiology*, *147*(3), 1437–1449. https://doi.org/10.1104/pp.108.119040

Doan, P. P. T., Vuong, H. H., & Kim, J. (2024). Genetic Foundation of Leaf Senescence: Insights from Natural and Cultivated Plant Diversity. *Plants (Basel, Switzerland)*, *13*(23). https://doi.org/10.3390/plants13233405

Edrisi Maryan, K., Farrokhi, N., & Samizadeh Lahiji, H. (2023). Cold-responsive transcription factors in Arabidopsis and rice: A regulatory network analysis using array data and gene co-expression network. *PloS One*, *18*(6), e0286324. https://doi.org/10.1371/journal.pone.0286324

Friedman, J., Hastie, T., & Tibshirani, R. (2010). Regularization paths for generalized linear models via coordinate descent. *Journal of Statistical Software*, *33*(1), 1.

Gaju, O., Allard, V., Martre, P., Le Gouis, J., Moreau, D., Bogard, M., Hubbart, S., & Foulkes, M. J. (2014). Nitrogen partitioning and remobilization in relation to leaf senescence, grain yield and grain nitrogen concentration in wheat cultivars. *Field Crops Research*, *155*, 213–223. https://doi.org/10.1016/j.fcr.2013.09.003

Gardner, J. C., Maranville, J. W., & Paparozzi, E. T. (1994). Nitrogen Use Efficiency among Diverse Sorghum Cultivars. *Crop Science*, *34*(3), 728–733. https://doi.org/10.2135/cropsci1994.0011183X003400030023x

Garnier, J., Billen, G., Aguilera, E., Lassaletta, L., Einarsson, R., Serra, J., Cameira, M. do R., Marques-Dos-Santos, C., & Sanz-Cobena, A. (2023). How much can changes in the agro-food system reduce agricultural nitrogen losses to the environment? Example of a temperate-Mediterranean gradient. *Journal of Environmental Management*, *337*, 117732. https://doi.org/10.1016/j.jenvman.2023.117732

Gelli, M., Konda, A. R., Liu, K., Zhang, C., Clemente, T. E., Holding, D. R., & Dweikat, I. M. (2017). Validation of QTL mapping and transcriptome profiling for identification of candidate genes associated with nitrogen stress tolerance in sorghum. *BMC Plant Biology*, *17*(1), 1–18. https://doi.org/10.1186/s12870-017-1064-9

Ge, Y., Bai, G., Stoerger, V., & Schnable, J. C. (2016). Temporal dynamics of maize plant growth, water use, and leaf water content using automated high throughput RGB and hyperspectral imaging. *Computers and Electronics in Agriculture*, *127*, 625–632. https://doi.org/10.1016/j.compag.2016.07.028

Govindasamy, P., Muthusamy, S. K., Bagavathiannan, M., Mowrer, J., Jagannadham, P. T. K., Maity, A., Halli, H. M., G K, S., Vadivel, R., T K, D., Raj, R., Pooniya, V., Babu, S., Rathore, S. S., L, M., & Tiwari, G. (2023). Nitrogen use efficiency-a key to enhance crop productivity under a changing climate. *Frontiers in Plant Science*, *14*, 1121073.

https://doi.org/10.3389/fpls.2023.1121073

Gregersen, P. L., Holm, P. B., & Krupinska, K. (2008). Leaf senescence and nutrient remobilisation in barley and wheat. *Plant Biology (Stuttgart, Germany)*, *10 Suppl 1*, 37–49. https://doi.org/10.1111/j.1438-8677.2008.00114.x

Gu, W., Feng, Y., Liu, C., Shi, X., Han, L., Liu, C., & Zhou, Y. (2025). Transcriptomic and metabolomic unraveling of nitrogen use efficiency in sorghum: the quest for molecular adaptations to low-nitrogen stress. *Plant Growth Regulation*, *105*(3), 687–706. https://doi.org/10.1007/s10725-025-01296-5

Hajibarat, Z., & Saidi, A. (2022). Senescence-associated proteins and nitrogen remobilization in grain filling under drought stress condition. *Journal, Genetic Engineering & Biotechnology*, *20*(1), 101. https://doi.org/10.1186/s43141-022-00378-5

Hao, B., Xie, Q., Bean, B. W., Rooney, W. L., & Becker, J. D. (2014). Biomass production, water and nitrogen use efficiency in photoperiod-sensitive sorghum in the Texas High Plains. *Biomass and Bioenergy*, *62*, 108–116. https://doi.org/10.1016/j.biombioe.2014.01.008

Hawkesford, M. J., & Griffiths, S. (2019). Exploiting genetic variation in nitrogen use efficiency for cereal crop improvement. *Current Opinion in Plant Biology*, *49*, 35–42. https://doi.org/10.1016/j.pbi.2019.05.003

Hirel, B., Andrieu, B., Valadier, M.-H., Renard, S., Quilleré, I., Chelle, M., Pommel, B., Fournier, C., & Drouet, J.-L. (2005). Physiology of maize II: Identification of physiological markers representative of the nitrogen status of maize (*Zea mays*) leaves during grain filling. *Physiologia Plantarum*, *124*(2), 178–188. https://doi.org/10.1111/j.1399-3054.2005.00511.x

Huynh-Thu, V. A., Irrthum, A., Wehenkel, L., & Geurts, P. (2010). Inferring regulatory networks from expression data using tree-based methods. *PloS One*, *5*(9). https://doi.org/10.1371/journal.pone.0012776

Karatzoglou, A., Smola, A., Hornik, K., & Zeileis, A. (2004). kernlab -- An S4 Package for Kernel Methods in R. *Journal of Statistical Software*, *11*(9), 1–20. http://www.jstatsoft.org/v11/i09/

Kuhn, M. (2020). *caret: Classification and Regression Training*. https://CRAN.R-project.org/package=caret

LeBauer, D., Maxwell, B., Demieville, J., Fahlgren, N., French, A., Garnett, R., Hu, Z., Huynh, K., Kooper, R., Li, Z., Maimaitijiang, M., Mao, J., Mockler, T., Morris, G., Newcomb, M., Ottman, M., Ozersky, P., Paheding, S., Pauli, D., … Zender, C. (2020). *Data From: TERRA-REF, An open reference data set from high resolution genomics, phenomics, and imaging sensors* [Dataset]. Dryad. https://doi.org/10.5061/DRYAD.4B8GTHT99

Liang, G., Hua, Y., Chen, H., Luo, J., Xiang, H., Song, H., & Zhang, Z. (2023). Increased nitrogen use efficiency via amino acid remobilization from source to sink organs in Brassica napus. *The Crop Journal*, *11*(1), 119–131. https://doi.org/10.1016/j.cj.2022.05.011

Li, B., & Dewey, C. N. (2011). RSEM: accurate transcript quantification from RNA-Seq data with or without a reference genome. *BMC Bioinformatics*, *12*(1), 323. https://doi.org/10.1186/1471-2105-12-323

Li, P., Li, X., & Jiang, M. (2021). CRISPR/Cas9-mediated mutagenesis of WRKY3 and WRKY4 function decreases salt and Me-JA stress tolerance in Arabidopsis thaliana. *Molecular Biology Reports*, *48*(8), 5821–5832. https://doi.org/10.1007/s11033-021-06541-4

Liu, G., & Godwin, I. D. (2012). Highly efficient sorghum transformation. *Plant Cell Reports*, *31*(6), 999–1007. https://doi.org/10.1007/s00299-011-1218-4

Mălinaş, A., Vidican, R., Rotar, I., Mălinaş, C., Moldovan, C. M., & Proorocu, M. (2022). Current Status and Future Prospective for Nitrogen Use Efficiency in Wheat (L.). *Plants (Basel, Switzerland)*, *11*(2). https://doi.org/10.3390/plants11020217

Masclaux-Daubresse, C., Carrayol, E., & Valadier, M.-H. (2005). The two nitrogen mobilisation-and senescence-associated GS1 and GDH genes are controlled by C and N

metabolites. *Planta*, *221*(4), 580–588.

Masclaux-Daubresse, C., Daniel-Vedele, F., Dechorgnat, J., Chardon, F., Gaufichon, L., & Suzuki, A. (2010). Nitrogen uptake, assimilation and remobilization in plants: challenges for sustainable and productive agriculture. *Annals of Botany*, *105*(7), 1141–1157.

Mercatelli, D., Scalambra, L., Triboli, L., Ray, F., & Giorgi, F. M. (2020). Gene regulatory network inference resources: A practical overview. *Biochimica et Biophysica Acta. Gene Regulatory Mechanisms*, *1863*(6), 194430. https://doi.org/10.1016/j.bbagrm.2019.194430

Mevik, B.-H., & Wehrens, R. (2007). The pls Package: Principal Component and Partial Least Squares Regression in R. *Journal of Statistical Software*, *18*, 1–23. https://doi.org/10.18637/jss.v018.i02

Mevik, B.-H., Wehrens, R., & Liland, K. H. (2020). *pls: Partial Least Squares and Principal Component Regression* (Version R package version 2.7-3). https://CRAN.R-project.org/package=pls

Miao, C., Pages, A., Xu, Z., Rodene, E., Yang, J., & Schnable, J. C. (2020). Semantic Segmentation of Sorghum Using Hyperspectral Data Identifies Genetic Associations. *Plant Phenomics (Washington, D.C.)*, *2020*, 4216373. https://doi.org/10.34133/2020/4216373

Price, M. N., & Arkin, A. P. (2017). PaperBLAST: Text Mining Papers for Information about Homologs. *mSystems*, *2*(4). https://doi.org/10.1128/mSystems.00039-17

Propheter, J. L., & Staggenborg, S. (2010). Performance of Annual and Perennial Biofuel Crops: Nutrient Removal during the First Two Years. *Agronomy Journal*, *102*(2), 798–805. https://doi.org/10.2134/agronj2009.0462

Qiao, Z., Li, C.-L., & Zhang, W. (2016). WRKY1 regulates stomatal movement in drought-stressed Arabidopsis thaliana. *Plant Molecular Biology*, *91*(1-2), 53–65. https://doi.org/10.1007/s11103-016-0441-3

Ram, B. G., Oduor, P., Igathinathane, C., Howatt, K., & Sun, X. (2024). A systematic review of hyperspectral imaging in precision agriculture: Analysis of its current state and future

prospects. *Computers and Electronics in Agriculture*, *222*(109037), 109037. https://doi.org/10.1016/j.compag.2024.109037

Rooney, W. L., Blumenthal, J., Bean, B., & Mullet, J. E. (2007). Designing sorghum as a dedicated bioenergy feedstock. *Biofuels, Bioproducts & Biorefining*, *1*(2), 147–157. https://doi.org/10.1002/bbb.15

Shanks, C. M., Huang, J., Cheng, C.-Y., Shih, H.-J. S., Brooks, M. D., Alvarez, J. M., Araus, V., Swift, J., Henry, A., & Coruzzi, G. M. (2022). Validation of a high-confidence regulatory network for gene-to-NUE phenotype in field-grown rice. *Frontiers in Plant Science*, *13*, 1006044. https://doi.org/10.3389/fpls.2022.1006044

Tran, T., Le, U., & Shi, Y. (2022). An effective up-sampling approach for breast cancer prediction with imbalanced data: A machine learning model-based comparative analysis. *PloS One*, *17*(5), e0269135. https://doi.org/10.1371/journal.pone.0269135

Trapnell, C., Williams, B. a., Pertea, G., Mortazavi, A., Kwan, G., van Baren, M. J., Salzberg, S. L., Wold, B. J., & Pachter, L. (2011). Transcript assembly and abundance estimation from RNA-Seq reveals thousands of new transcripts and switching among isoforms. *Nature Biotechnology*, *28*(5), 511–515. https://doi.org/10.1038/nbt.1621.Transcript

Venables, W. N., & Ripley, B. D. (2002). *Modern Applied Statistics with S* (Fourth). Springer. http://www.stats.ox.ac.uk/pub/MASS4/

Wagstaff, C., Yang, T. J. W., Stead, A. D., Buchanan-Wollaston, V., & Roberts, J. A. (2009). A molecular and structural characterization of senescing Arabidopsis siliques and comparison of transcriptional profiles with senescing petals and leaves. *The Plant Journal : For Cell and Molecular Biology*, *57*(4), 690–705. https://doi.org/10.1111/j.1365-313X.2008.03722.x

Wingler, A., Marès, M., & Pourtau, N. (2004). Spatial patterns and metabolic regulation of photosynthetic parameters during leaf senescence. *The New Phytologist*, *161*(3), 781–789.

https://doi.org/10.1111/j.1469-8137.2004.00996.x

Woo, H. R., Masclaux-Daubresse, C., & Lim, P. O. (2018). Plant senescence: how plants know when and how to die. *Journal of Experimental Botany*, *69*(4), 715–718. https://doi.org/10.1093/jxb/ery011

Wu, T. D., & Nacu, S. (2010). Fast and SNP-tolerant detection of complex variants and splicing in short reads. *Bioinformatics* , *26*(7), 873–881. https://doi.org/10.1093/bioinformatics/btq057

Yang, J., & Zhang, J. (2006). Grain filling of cereals under soil drying. *The New Phytologist*, *169*(2), 223–236. https://doi.org/10.1111/j.1469-8137.2005.01597.x

Zhang, L., & Becker, D. F. (2015). Connecting proline metabolism and signaling pathways in plant senescence. *Frontiers in Plant Science*, *6*, 552. https://doi.org/10.3389/fpls.2015.00552

Zhang, W., Tang, S., Li, X., Chen, Y., Li, J., Wang, Y., Bian, R., Jin, Y., Zhu, X., & Zhang, K. (2024). Arabidopsis WRKY1 promotes monocarpic senescence by integrative regulation of flowering, leaf senescence, and nitrogen remobilization. *Molecular Plant*, *17*(8), 1289–1306. https://doi.org/10.1016/j.molp.2024.07.005

Zheng, H., Dang, Y., & Sui, N. (2023). Sorghum: A multipurpose crop. *Journal of Agricultural and Food Chemistry*, *71*(46), 17570–17583. https://doi.org/10.1021/acs.jafc.3c04942

Supplementary Files

This is a list of supplementary files associated with this preprint. Click to download.

- Highthroughputhyperspectralphenotypingandtranscriptomicsrevealexpressionnetworksassociatedwithnitrogenlimitationinducedsenescenceinsorghums